ACCEPTED: Biological Psychiatry

Supplementary Online Content

Dynamic Alterations in Neural Networks Supporting Aversive Learning in Children Exposed to Trauma: Neural Mechanisms Underlying Psychopathology

Stephanie N. DeCross, M.A. [1], Kelly A. Sambrook, M.S. [2], Margaret A. Sheridan, Ph.D. [3], Nim Tottenham Ph.D. [4], & Katie A. McLaughlin, Ph.D. [1]

[1] Department of Psychology, Harvard University, Cambridge, MA
[2] Department of Radiology, University of Washington, Seattle, WA
[3] Department of Psychology and Neuroscience, University of North Carolina, Chapel Hill, NC
[4] Department of Psychology, Columbia University, New York, NY

Table of Contents

Supplementary Methods

Measures

Trauma Exposure. Inter-rater reliability was good between child and caregiver reports in the whole sample (82.0% agreement; kappa = 0.62). Within the trauma group, 5.2% had experienced physical abuse only, 13.0% sexual abuse only, 9.1% domestic violence only, and 72.7% a combination of these experiences.

Psychopathology. The CDI and SCARED are both self-report measures with sound psychometric properties (1,2) and excellent internal consistency in our sample ($\alpha = .89$, $\alpha = .94$, respectively). The PTSD-RI has sound psychometric properties (3) and excellent internal consistency in our sample ($\alpha = 0.92$). The Youth Self-Report/Child Behavior Checklist scales are among the most commonly used measures of youth emotional and behavioral problems and use extensive normative data to generate age-standardized estimates of symptom severity.

The highest score of the two reporters was used for PTSD and externalizing symptoms. This is an implementation of the standard "or" rule used in combining caregiver and child reports of psychopathology. In this approach, if either a caregiver or child endorses a particular symptom, it is counted with the assumption that if a symptom is reported, it is likely present. This is a standard approach in the child psychopathology literature; for example, it is how mental disorders are diagnosed in population-based studies of child and adolescent psychopathology (4,5).

Fear Conditioning Task. The task was a commonly-used Pavlovian differential fear conditioning paradigm (6). Instructions before the task included that the participant would "see some shapes on the screen while some sounds play." Each block lasted 20 seconds, and was presented for the first time in the following order and then pseudo-randomized thereafter: CS-, reinforced CS+ (CS+R), non-reinforced CS+ (CS+), and baseline/inter-trial interval (ITI). The CS-, CS+R, and CS+ blocks each consisted of ten 1500-ms CS presentations alternated with 500-ms fixation crosses. The CS co-terminated with a 300-ms US for 80% of the presentations during the CS+R blocks; the US did not occur during the non-reinforced CS+ blocks, which were included for use in analysis of response to the CS+ without the US confound.

Neuroimaging Acquisition and Preprocessing

Acquisition. Children 12 years and younger and older children exhibiting anxiety about the scan underwent a mock scan procedure (7). Inflatable head-stabilizing pillows were used during the scan to restrict movement. All images were acquired using a 3T Phillips Achieva scanner at the University of Washington Integrated Brain Imaging Center using a 32-channel head coil. Anatomical scans (T1-weighted MPRAGE volumes; repetition time (TR) = 2530 ms, echo time (TE) = 3.5 ms, flip angle = 7°, field of view (FOV) = 256 x 256, voxel size = 1 mm^3, 176 slices) were acquired for co-registration with functional magnetic resonance imaging (fMRI) data. Blood oxygenation level dependent (BOLD) signal during functional runs was acquired using a gradient-echo T2*-weighted echo planar imaging (EPI) sequence. Thirty-seven 3-mm-thick slices were acquired sequentially and parallel to the AC-PC line (TR = 2 s, TE = 25 ms, flip angle = 79°, FOV = 224 x 224, voxel size = 3 mm^3, inter-slice gap = 0.6 mm, matrix size = 76 x 74). Prior to each scan, 4 images were acquired and discarded to allow longitudinal magnetization to reach equilibrium.

Preprocessing. Data preprocessing was performed in a pipeline using Make, a software development tool that can be used to create neuroimaging workflows that rely on multiple

software packages (8). Preprocessing steps included motion correction with FSL MCFLIRT followed by slice-timing correction with FSL slicetimer (9), despiking with AFNI 3dDespike (10), and spatial smoothing with FSL SUSAN using a 6 mm full-width half-max Gaussian kernel (11). Nuisance regressors entered into individual-level models included 6 rigid-body motion parameters as well as timeseries extracted from white matter and ventricles to control for physiological noise (12). Outlier volumes in which framewise displacement exceeded 1 mm, the derivative of variance in BOLD signal across the brain (DVARS) exceeded the upper fence (above 75th percentile + 1.5 x inter-quartile range), or signal intensity was more than 3 SD from the mean were excluded by regressing these volumes out of individual-level models. There were 519 total frame outliers for the control group (M = 7.41, SD = 5.25; average of 4.6% frames) and 849 for the trauma group (M = 11.03, SD = 8.00; average of 6.9% frames), which was significantly different between groups (t(132.33) = -3.26, p = 0.001). Individual- and group-level models were estimated in FSL. Following estimation of the individual-level models, the resulting contrast images were registered to a custom study-specific template and then to standard MNI space. Anatomical co-registration of the functional data with each participant's T1-weighted image and normalization were performed using Advanced Normalization Tools (ANTs) (13).

Analyses

fMRI Whole-Brain Analysis. FSL's FLAME1 was used for estimating group level models (14). For all between-group whole-brain analyses, race/ethnicity (white vs. non-white) and income-to-needs ratio were included as covariates. Income-to-needs ratio was a continuous variable, and for 2 control group and 8 trauma group participants with missing data, the average income-to-needs ratio of each respective group was used, in order to retain all participants in these analyses.

MRIcroGL was used to visualize whole-brain findings (https://www.nitrc.org/projects/mricrogl).

Region-of-Interest Analyses. Subcortical ROIs were defined anatomically, using right and left amygdala and hippocampus ROIs from the Harvard-Oxford Atlas (50% threshold). Cortical ROIs were defined by masking meta-analytic clusters (15) including the dorsal anterior cingulate cortex (ACC), insula, parahippocampal gyrus (PHG), and ventromedial prefrontal cortex (vmPFC) to the following anatomical structures from the Harvard-Oxford Atlas (20% threshold): anterior cingulate gyrus, insula, posterior parahippocampal gyrus, and frontal medial cortex.

Mixed effects models using the lme4 package in R (16) included ROI neural response as the outcome measure; stimulus, block number, childhood trauma, and their interactions as predictors. A random intercept and a random slope of block were included in step-wise models and retained if they improved model fit via AIC (17). Race/ethnicity and income-to-needs covariates were entered as fixed effects. For significant models, we conducted additional analyses to determine whether age, sex, puberty stage (assessed with the Tanner scale), or an interaction between trauma and any of these variables predicted the pattern of neural response. Models were corrected for multiple comparisons using FDR-correction at the level of the hypothesis, correcting for 4 comparisons within each network (i.e., left and right amygdala, ACC, and insula for the salience network; left and right hippocampus, PHG, and vmPFC for the default mode network).

In the differential plots in Figure 2, Figure S3, and Figure S4, approximated slope lines are added for visualization purposes only.

Task-Based Functional Connectivity. In our generalized psychophysiology interaction (gPPI) analyses, the seed region selected was the right amygdala, due to its central involvement in

aversive learning (18). This anatomical ROI was created from the Harvard-Oxford Atlas (50% threshold), and timeseries were extracted of the average activity of all voxels in the ROI. Individual-level analyses were modeled as before, with the addition of 3 regressors for the seed timeseries and the interactions of the seed timeseries with task regressors for CS+ and CS-. In this kind of model, significant results represent task-dependent activity in voxels significantly correlated with right amygdala activity, over and above task-independent correlated activity. In other words, gPPI isolates which voxels are differentially functionally coupled with right amygdala during different phases of the task.

For extracting mean z-scores of connectivity from regions showing differential connectivity with right amygdala between groups, ROIs were defined as before and warped into native space. For subcortical regions, anatomical ROIs from the Harvard-Oxford Atlas (50% threshold) were used. To our knowledge, no meta-analysis of amygdala connectivity during fear conditioning has been performed, so cortical ROIs were conservatively based on meta-analytic results of activity during fear conditioning, as before. For the cortical regions showing differential connectivity (ACC, PHG, precuneus/posterior cingulate cortex (PCC)), meta-analytic clusters (15) including these regions were masked to the following anatomical structures, respectively, from the Harvard-Oxford Atlas (20% threshold): anterior cingulate gyrus, posterior parahippocampal gyrus, and a combined mask of precuneus and PCC, which were merged to best capture the localization evidenced by the meta-analytic results. For these regions, we conducted additional analyses to determine whether age, sex, puberty stage (assessed with the Tanner scale), or an interaction between trauma and any of these variables predicted connectivity.

Psychopathology. Because most psychopathology outcome measures were heavily right-skewed, regression models were computed using underlying assumptions of both normal and negative binomial distributions, and the model of best fit was selected according to AIC. Of note, parameter estimates of negative binomial models are not directly comparable to those of models with underlying assumptions of normal distributions and are interpreted as follows: for a one-unit change in the predictor variable, the difference in logs of expected counts of the outcome variable will change by the coefficient. Techniques to model mediations with different branches using normal and negative binomial distributions are unavailable, and therefore mediation models were fit with the underlying assumption of normal distributions for all branches.

To examine whether changing neural activation over time predicted psychopathology, we fit a linear regression to the ROI data of each participant and used the linear beta value (slope) across blocks as the predictor. For the ROIs typically more activated to CS+ than CS- during fear conditioning (amygdala, insula, ACC) (15), the slope across blocks of differential response to CS+ vs. CS- was computed. This resulted in "habituation slopes," and these slopes were typically negative (i.e., decreasing activation to the threat cue over time). For ROIs typically more activated to CS- than CS+ (hippocampus, PHG, vmPFC) (15), the slope across blocks of differential response to CS- vs. CS+ was computed. This resulted in "safety-signaling slopes," and these slopes were typically positive (i.e., increasing activation to the safety cue over time). We refer to "habituation slopes" and "safety-signaling slopes" together under the umbrella term "learning slopes." Models testing whether neural measures predicted psychopathology symptoms were corrected for multiple comparisons using FDR-correction at the level of the hypothesis, correcting for 5 comparisons across forms of psychopathology symptoms (i.e., depression, generalized anxiety, panic, PTSD, and externalizing symptoms).

Mediation models were run using the mediation package in R (19).

Supplementary Tables

Table S1. Clusters showing significant findings in whole-brain analyses in the whole group (n = 147)

Analysis	Regions	x	y	z	p-value	z-max	Voxels
(A) Overall Task Effects							
CS+ > CS-	Precentral gyrus, postcentral gyrus, anterior cingulate gyrus, paracingulate gyrus, opercular cortex, insular cortex, middle temporal gyrus, superior temporal gyrus, supplementary motor cortex, frontal pole, parahippocampal gyrus, thalamus	-50	2	-6	< .001	7.31	23894
	Opercular cortex, middle temporal gyrus, superior temporal gyrus, insular cortex, postcentral gyrus, supramarginal gyrus, putamen, pallidum, amygdala	52	6	-4	< .001	5.53	7913
CS- > CS+	Fusiform cortex, superior lateral occipital cortex, inferior lateral occipital cortex, superior parietal lobe, intraparietal sulcus, occipital pole, inferior temporal gyrus, parahippocampal gyrus, hippocampus	-20	-66	34	< .001	5.78	12760
(B) Parametric Modulation Analyses							
Decreasing activation to CS+ > CS-, or increasing activation to CS- > CS+	Opercular cortex, lingual gyrus, fusiform cortex, middle temporal gyrus, superior temporal gyrus, temporal pole, insular cortex, frontal orbital cortex, subcallosal cortex, parahippocampal gyrus, brainstem, thalamus, amygdala, hippocampus	-60	-6	-2	< .001	7.10	25332
	Precentral gyrus, postcentral gyrus, superior parietal lobe, supplementary motor cortex, anterior cingulate gyrus, posterior cingulate gyrus, precuneus	-18	-50	58	< .001	5.10	7483
	Frontal pole, frontal medial cortex, paracingulate gyrus	2	60	12	< .001	5.17	3264
Increasing activation to CS+ > CS-, or decreasing activation to CS- > CS+	Superior lateral occipital cortex, inferior lateral occipital cortex, superior parietal lobe, intraparietal sulcus, angular gyrus	28	-64	32	< .001	5.29	3494
	Superior lateral occipital cortex, inferior lateral occipital cortex, superior parietal lobe, intraparietal sulcus, precuneus	-20	-66	32	< .001	5.78	2635
(C) Task-Based Functional Connectivity							
CS- > CS+	Cerebellum	14	-72	-28	< .001	4.04	2823

Information about clusters of activation from each whole-brain analysis in the whole group is listed. In C, no findings in the CS+ > CS- contrast were observed.

Table S2. Clusters showing significant findings in whole-brain comparisons of the trauma group (n = 77) and control group (n = 70)

Analysis	Regions	x	y	z	p-value	z-max	Voxels
(A) Task-Based Functional Connectivity							
Control > Trauma							
CS+ > CS-	Hippocampus, precuneus, posterior cingulate cortex, posterior parahippocampal gyrus, fusiform cortex, lingual gyrus	-14	-36	-12	< .001	3.89	6679
Trauma > Control							
CS+ > CS-	Postcentral gyrus, precentral gyrus, supplementary motor cortex, anterior cingulate cortex, superior lateral occipital cortex, superior parietal lobe	-16	-48	44	< .001	3.86	5194

No findings were observed in the between-group comparisons of overall task effects averaged across the whole run or parametric modulation analyses. In A, redundant contrasts are not listed.

Supplementary Figures

Figure S1. Task diagram

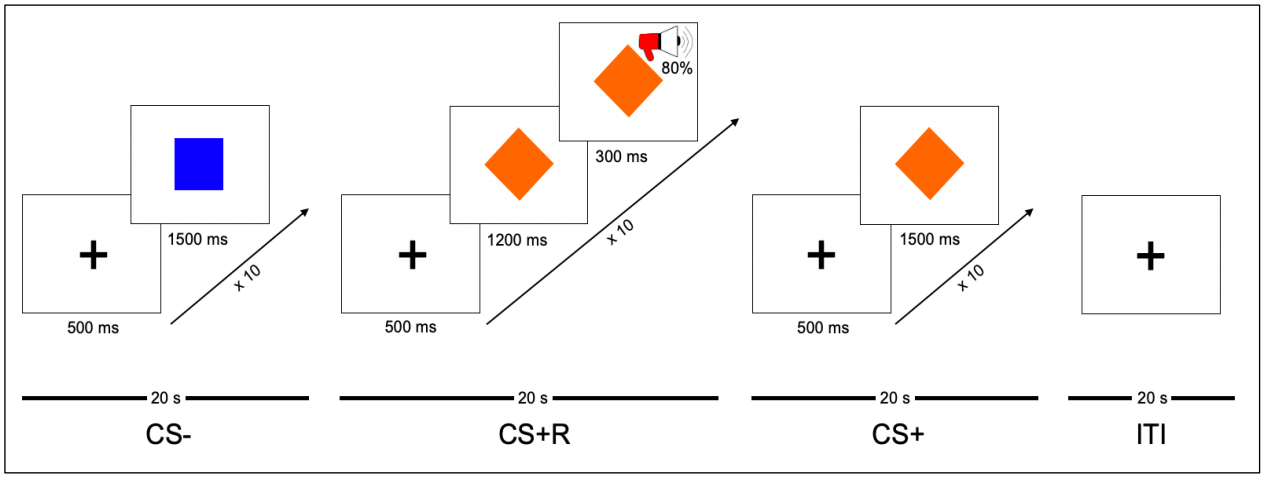

Schematic of the fear conditioning paradigm, commonly used in developmental samples (6). Each of the four types of blocks (CS-, reinforced CS+ (CS+R), non-reinforced CS+ (CS+), and baseline/inter-trial interval (ITI)) were pseudo-randomly presented 4 times each. See Supplementary Methods for further detail.

Figure S2. ROIs used in the dynamic learning analyses

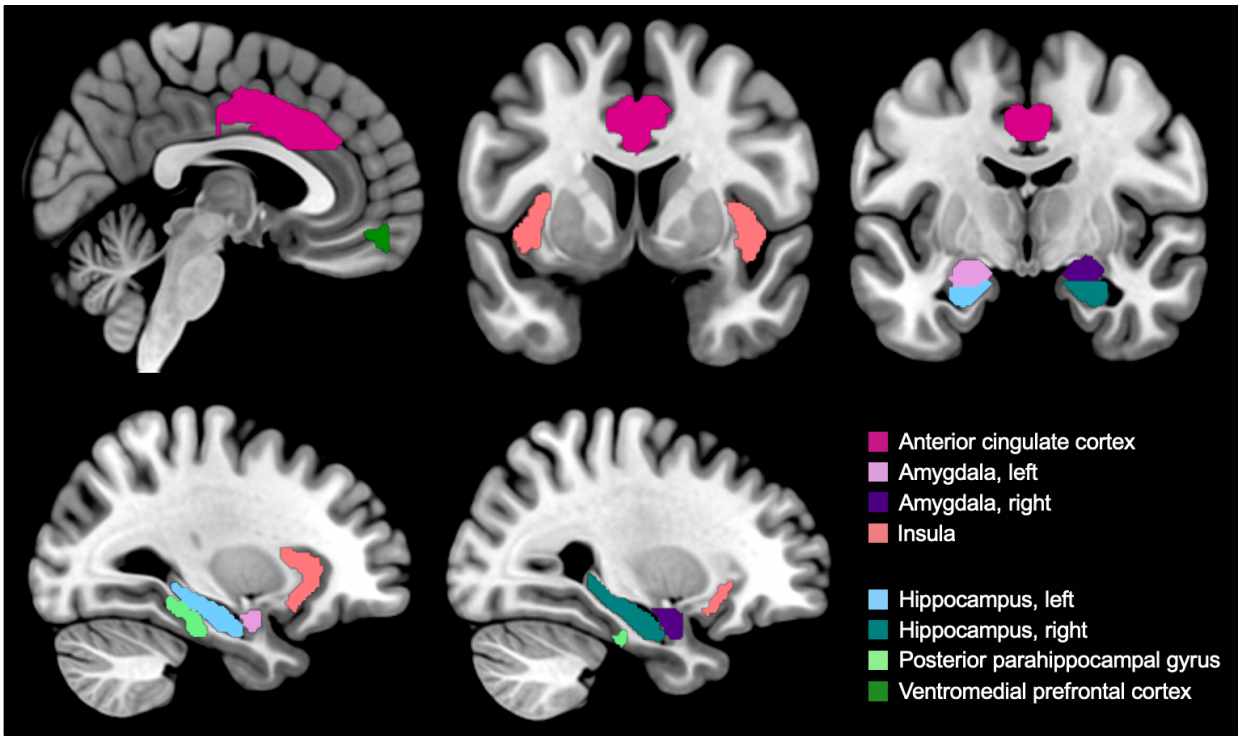

ROIs used in the dynamic fear conditioning analyses. Subcortical ROIs are anatomically defined; cortical ROIs are defined from anatomically-constrained meta-analytic results. Slice selection clockwise from top left: x = 3, y = 5, y = -8, x = 28, x = -30.

Figure S3. Additional ROI findings

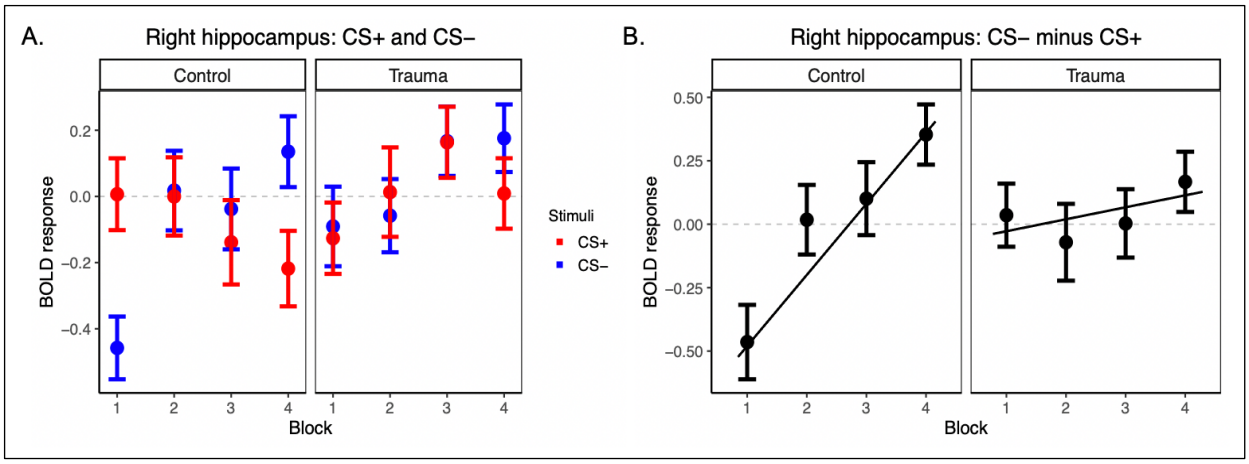

Though these results did not survive correction for multiple comparisons, the difference in patterns of activation over time between the two groups in right hippocampus is similar to the observed, significant pattern in right amygdala, with the trauma group displaying blunted learning slopes. Learning slopes are plotted for CS- minus CS+ because the hippocampus is typically activated to CS- > CS+; such slopes reflect intact or blunted slopes of safety-signaling over time.

The salience and default mode networks are regarded as playing opposite roles during fear conditioning (i.e., typically activated to either CS+ > CS- or CS- > CS+ when averaged across the task). However, notable similarities appear in dynamic activation patterns across these regions. As shown in Figure 2A in the main manuscript and in Figure S3A above, regions across both networks demonstrate similar patterns of dynamic response over time, with decreasing activation to the threat cue and increasing activation to the safety cue. The tendency of salience network regions to be activated to CS+ > CS- and default mode network regions to be activated to CS- > CS+ when averaged across the task may be a reflection of the *degree* of these patterns, rather than an overall difference in shape of patterns of activation.

Figure S4. US-related ROI analyses

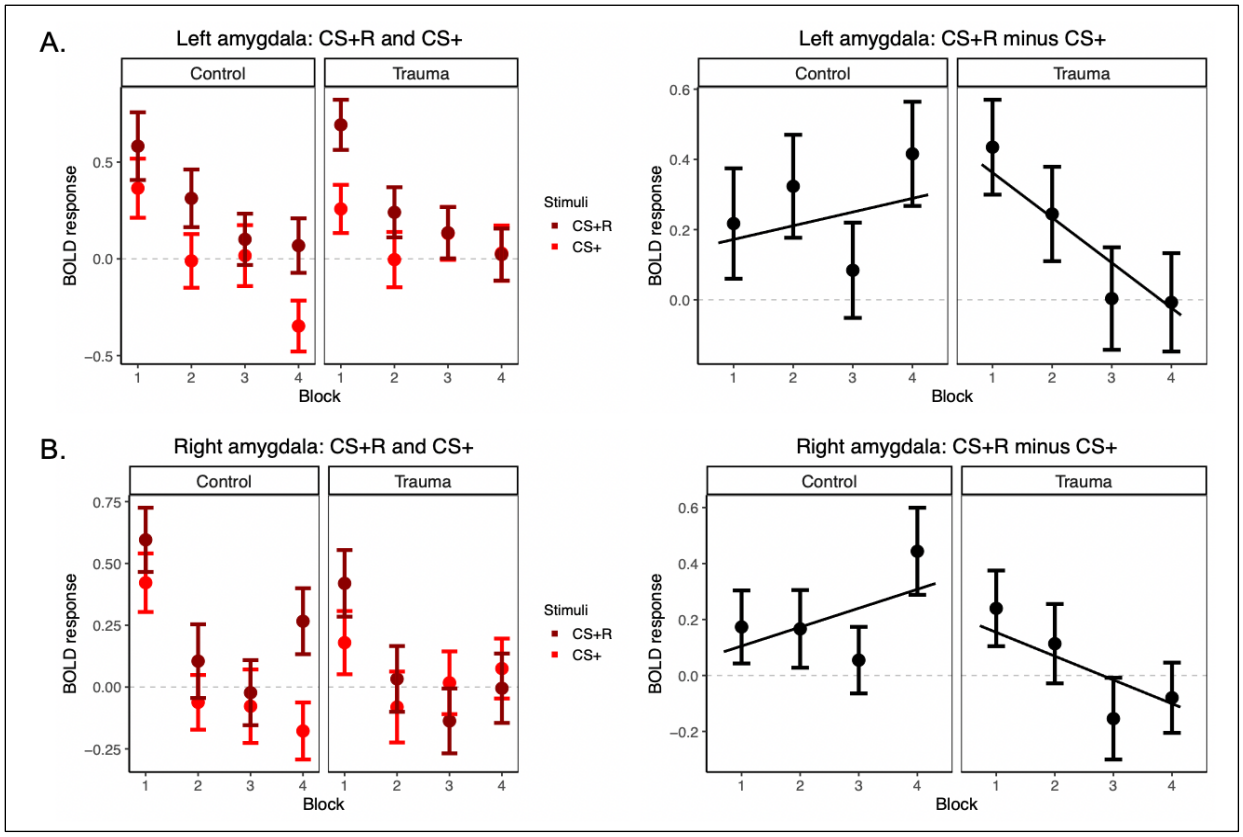

We conducted an ROI investigation to determine whether there were group differences in response to the unconditioned stimulus (US) by comparing the reinforced CS+ blocks (CS+R) and non-reinforced CS+ blocks (CS+) over time (left panels) and isolating the responses to the US (right panels). Mixed effects models showed that dynamic responses to the US were not significantly different between groups for the left (X^2 (1, N = 147) = 3.36, p = .07) or right (X^2 (1, N = 147) = 3.57, p = .07) amygdala, corrected for multiple comparisons. The observed pattern appears more related to a late elevation in US response differential in the control group, rather than an early blunted US response or more rapid habituation response to the US in the trauma group.

Figure S5. Alternative visualization of functional connectivity

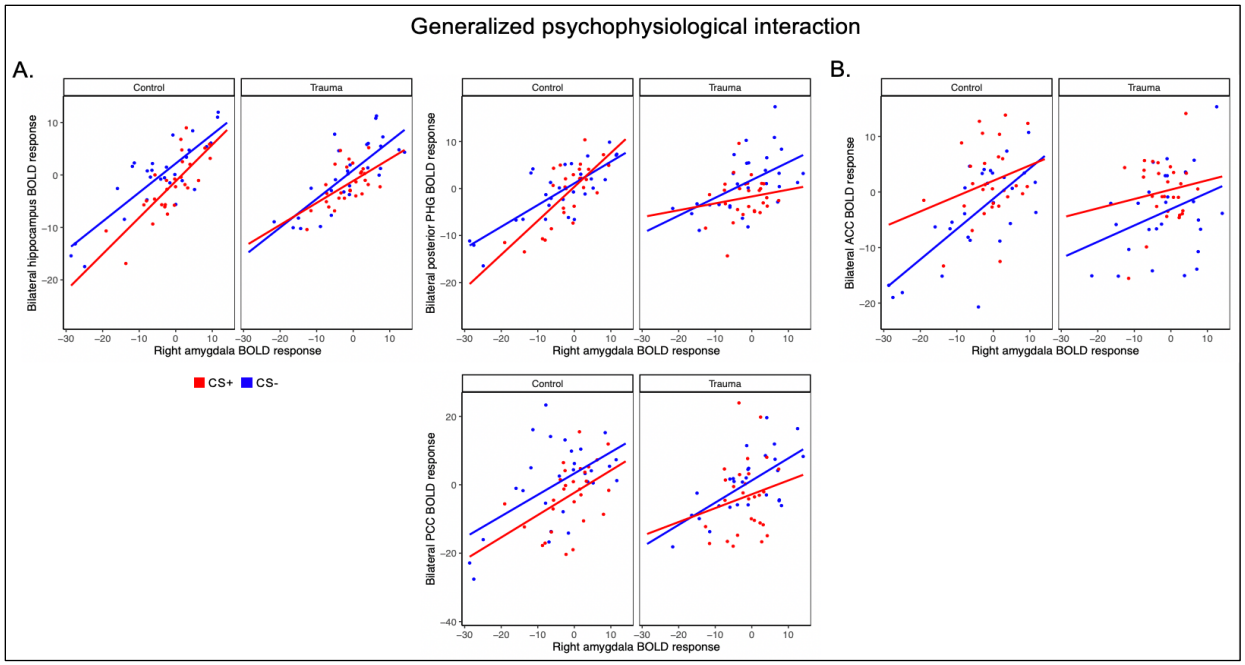

An alternative visualization of functional connectivity (20). To create the plots in this figure, activation from subcortical regions was extracted from Harvard-Oxford Atlas anatomical ROIs (50% threshold); for cortical regions, anatomically-constrained meta-analytic ROIs were used. By plotting the activation in the seed region (right amygdala) against the target region at each TR during each phase of the task, it becomes possible to visualize both the direction of the connectivity relationship (positive slopes correspond to positive functional coupling; negative slopes correspond to negative functional coupling) as well as to compare the relative strength of connectivity during different tasks (steeper slopes of higher absolute value magnitude correspond to a greater strength of functional coupling; the intercept does not carry meaning). Note that these interpretations may not be validly drawn from the findings in Figure 3 in the main manuscript alone, which depict overall interactions without specifying the conditions under which these interactions arise.

The plots in A expand upon the results in Figure 3A in the main manuscript that demonstrate that the trauma group compared to the control group showed reduced connectivity of right amygdala with bilateral hippocampus, parahippocampal gyrus, and posterior cingulate cortex during CS+ > CS-. Here, A demonstrates that the group differences visualized by the interaction depicted in Figure 3A in the main manuscript arise from a blunted strength of functional connectivity between right amygdala and these regions in the trauma group compared to the control group during the CS+ (indicated by the blunted, flatter CS+ slopes in the trauma compared to control group), while the strength of functional connectivity during CS- is comparable between groups (indicated by similar CS- slopes for each group).

The plots in B expand upon the results in Figure 3B in the main manuscript that demonstrate that the trauma group compared to the control group showed elevated connectivity of right amygdala with bilateral anterior cingulate cortex and other fronto-parietal regions associated with attentional direction and initiation of defensive responses during CS+ > CS-. Here, B demonstrates that the group difference visualized by the interaction depicted in Figure 3B in the main manuscript result from similar magnitude of functional connectivity of right amygdala with these regions regardless of the task phase in the trauma group (indicated by more similar CS+ and CS- slopes in the trauma group), while the control group exhibits a greater degree of task-dependent functional coupling. ACC, anterior cingulate cortex; PHG, parahippocampal gyrus; PCC, posterior cingulate cortex (and precuneus, as described in Supplementary Methods).

Figure S6. Functional connectivity to CS+ > CS- by sex interactions

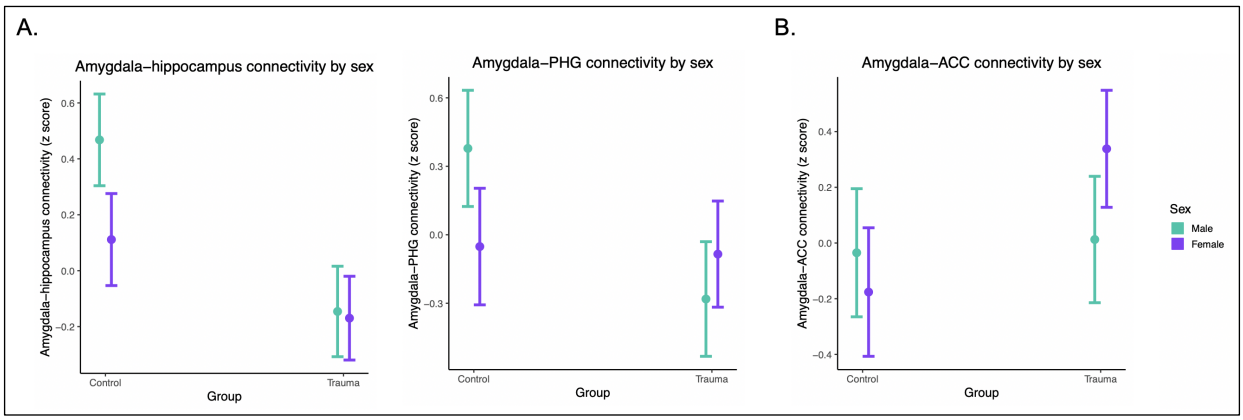

In A, a trauma x sex interaction predicted functional connectivity during CS+ > CS- between the amygdala and hippocampus (b= .33, p = .030) and parahippocampal gyrus (PHG, b = .63, p = .010). Regardless of sex, trauma-exposed participants exhibited reduced amygdala-hippocampus and amygdala-PHG connectivity. In controls, females had lower connectivity compared to males. In B, a trauma x sex interaction also predicted functional connectivity during CS+ > CS- between the amygdala and anterior cingulate cortex (ACC, b = .47, p = .030), such that connectivity was elevated specifically among trauma-exposed females.

Supplementary References

1. Craighead WE, Smucker MR, Craighead LW, Ilardi SS (1998): Factor analysis of the Children's Depression Inventory in a community sample. *Psychol Assess* 10: 156.

2. Birmaher B, Brent DA, Chiappetta L, Bridge J, Monga S, Baugher M (1999): Psychometric Properties of the Screen for Child Anxiety Related Emotional Disorders (SCARED): A Replication Study. *J Am Acad Child Adolesc Psychiatry* 38: 1230–1236.

3. Steinberg AM, Brymer MJ, Kim S, Briggs EC, Ippen CG, Ostrowski SA, *et al.* (2013): Psychometric properties of the UCLA PTSD Reaction Index: Part I. *J Trauma Stress* 26: 1–9.

4. Kessler RC, Avenevoli S, Costello EJ, Georgiades K, Green JG, Gruber MJ, *et al.* (2012): Prevalence, Persistence, and Sociodemographic Correlates of DSM-IV Disorders in the National Comorbidity Survey Replication Adolescent Supplement. *Arch Gen Psychiatry* 69: 372–380.

5. Merikangas KR, He J-P, Burstein M, Swanson SA, Avenevoli S, Cui L, *et al.* (2010): Lifetime prevalence of mental disorders in U.S. adolescents: results from the National Comorbidity Survey Replication--Adolescent Supplement (NCS-A). *J Am Acad Child Adolesc Psychiatry* 49: 980–989.

6. Silvers JA, Lumian DS, Gabard-Durnam L, Gee DG, Goff B, Fareri DS, *et al.* (2016): Previous Institutionalization Is Followed by Broader Amygdala–Hippocampal–PFC Network Connectivity during Aversive Learning in Human Development. *J Neurosci* 36: 6420–6430.

7. Raschle N, Zuk J, Ortiz-Mantilla S, Sliva DD, Franceschi A, Grant PE, *et al.* (2012): Pediatric neuroimaging in early childhood and infancy: challenges and practical guidelines. *Ann N Y Acad Sci* 1252: 43–50.

8. Askren MK, McAllister-Day TK, Koh N, Mestre Z, Dines JN, Korman BA, *et al.* (2016): Using Make for Reproducible and Parallel Neuroimaging Workflow and Quality-Assurance. *Front Neuroinformatics* 10: 2.

9. Jenkinson M, Bannister P, Brady M, Smith S (2002): Improved optimization for the robust and accurate linear registration and motion correction of brain images. *NeuroImage* 17: 825–841.

10. Cox RW (1996): AFNI: software for analysis and visualization of functional magnetic resonance neuroimages. *Comput Biomed Res Int J* 29: 162–173.

11. Smith SM, Brady JM (1997): SUSAN—A New Approach to Low Level Image Processing. 34.

12. Behzadi Y, Restom K, Liau J, Liu TT (2007): A component based noise correction method (CompCor) for BOLD and perfusion based fMRI. *NeuroImage* 37: 90–101.

13. Avants BB, Tustison NJ, Song G, Cook PA, Klein A, Gee JC (2011): A reproducible evaluation of ANTs similarity metric performance in brain image registration. *NeuroImage* 54: 2033–2044.

14. Jenkinson M, Beckmann CF, Behrens TEJ, Woolrich MW, Smith SM (2012): FSL. *NeuroImage* 62: 782–790.

15. Fullana MA, Harrison BJ, Soriano-Mas C, Vervliet B, Cardoner N, Àvila-Parcet A, Radua J (2016): Neural signatures of human fear conditioning: an updated and extended meta-analysis of fMRI studies. *Mol Psychiatry* 21: 500–508.

16. Bates D, Mächler M, Bolker B, Walker S (2015): Fitting Linear Mixed-Effects Models Using **lme4**. *J Stat Softw* 67. https://doi.org/10.18637/jss.v067.i01

17. Akaike H (1973): Information theory as an extension of the maximum likelihood principle. Á In: Petrov, BN and Csaki, F. *Second International Symposium on Information Theory. Akademiai Kiado, Budapest, Pp. 276Á281*.

18. LaBar KS, Gatenby JC, Gore JC, LeDoux JE, Phelps EA (1998): Human Amygdala Activation during Conditioned Fear Acquisition and Extinction: a Mixed-Trial fMRI Study. *Neuron* 20: 937–945.

19. Tingley D, Yamamoto T, Hirose K, Keele L, Imai K (2014): **mediation** : *R* Package for Causal Mediation Analysis. *J Stat Softw* 59. https://doi.org/10.18637/jss.v059.i05

20. Friston KJ, Buechel C, Fink GR, Morris J, Rolls E, Dolan RJ (1997): Psychophysiological and modulatory interactions in neuroimaging. *NeuroImage* 6: 218–229.